The photosynthetic cytochrome c_{550} from the diatom *Phaeodactylum tricornutum*

Pilar BERNAL-BAYARD[1], Leonor PUERTO-GALÁN[1], Inmaculada YRUELA[2], Inés GARCÍA-RUBIO[3,4], Carmen CASTELL[1], José M. ORTEGA[1], Pablo J. ALONSO[5], Mercedes RONCEL[1], Jesús I. MARTÍNEZ[3,5], Manuel HERVÁS[1], José A. NAVARRO[1*]

[1]Instituto de Bioquímica Vegetal y Fotosíntesis, cicCartuja, Universidad de Sevilla & CSIC, Sevilla, Spain.

[2]Estación Experimental de Aula Dei, EEAD-CSIC, Zaragoza, Spain.

[3]Centro Universitario de la Defensa, Zaragoza, Spain.

[4]Laboratory of Physical Chemistry, ETH Zurich, Switzerland.

[5]Instituto de Ciencia de Materiales de Aragón, Universidad de Zaragoza & CSIC, Zaragoza, Spain.

*Corresponding author: José A. Navarro, Instituto de Bioquímica Vegetal y Fotosíntesis, Centro de Investigaciones Científicas Isla de la Cartuja, Universidad de Sevilla & CSIC, Américo Vespucio 49, 41092-Sevilla, Spain. Fax: +34 954460165; E-mail: jnavarro@ibvf.csic.es

KEY WORDS: cytochrome c_{550}, *Phaeodactylum*, photosystem II, EPR, hemeprotein

Funding:

This work was supported by the Spanish Ministry of Economy and Competitiveness (BIO2012-35271, BIO2015-64169-P, MAT2011-23861 and CTQ2015-64486-R) the Andalusian Government (PAIDI BIO-022) and the Aragón Government (Grupo consolidado B-18). All these grants were partially financed by the EU FEDER Program.

Abbreviations:

ß-DM, ß-dodecyl-maltoside; Cc_{550}, cytochrome c_{550}; Cc_6, cytochrome c_6; CW, continuous wave; EPR, electron paramagnetic resonance; HYSCORE, hyperfine sublevel correlation spectroscopy; MALDI-TOF MS, Matrix-Assisted Laser Desorption/Ionization Time-of-Flight Mass Spectrometry; PSII, photosystem II.

ABSTRACT

The photosynthetic cytochrome c_{550} from the marine diatom *Phaeodactylum tricornutum* has been purified and characterized. Cytochrome c_{550} is mostly obtained from the soluble cell extract in relatively large amounts. In addition, the protein appeared to be truncated in the last hydrophobic residues of the C-terminus, both in the soluble cytochrome c_{550} and in the protein extracted from the membrane fraction, as deduced by mass spectrometry analysis and the comparison with the gene sequence. Interestingly, it has been described that the C-terminus of cytochrome c_{550} forms a hydrophobic finger involved in the interaction with photosystem II in cyanobacteria. Cytochrome c_{550} was almost absent in solubilized photosystem II complex samples, in contrast with the PsbO and Psb31 extrinsic subunits, thus suggesting a lower affinity of cytochrome c_{550} for the photosystem II complex. Under iron-limiting conditions the amount of cytochrome c_{550} decreases up to about 45% as compared to iron-replete cells, pointing to an iron-regulated synthesis. Oxidized cytochrome c_{550} has been characterized using continuous wave EPR and pulse techniques, including HYSCORE, and the obtained results have been interpreted in terms of the electrostatic charge distribution in the surroundings of the heme centre.

INTRODUCTION

Photosynthetic cytochrome c_{550} (Cc_{550}) is a *c*-type heme protein with a very unusual bis-histidinyl axial coordination (Frazão et al. 2001). It is currently accepted that Cc_{550} is an extrinsic protein subunit of photosystem II (PSII), since it appears stoichiometrically bound to the luminal PSII surface in the vicinity of the D1 and CP43 proteins, and close to the oxygen evolving complex (Zouni et al. 2001; Ferreira et al. 2004; Umena et al. 2011; Shen 2015; Ago et al. 2016). Cc_{550} is present in cyanobacteria and in eukaryotic algae from the red photosynthetic lineage, which includes diatoms, but is absent in the green lineage, which comprises green algae and plants, which seem to have replaced Cc_{550} for the non-iron containing PsbP subunit (revised in: Enami et al. 2008; Roncel et al. 2012; Ifuku and Noguchi 2016).

The role of Cc_{550} in PSII appears to be stabilizing the Mn_4CaO_5 cluster and the binding of Cl^- and Ca^{2+} ions (Shen and Inoue 1993; Enami et al. 1998, 2008; Kerfeld and Krogmann 1998; Shen et al. 1998; Nagao et al. 2010a,b; Bricker et al. 2012). Crystal structures and theoretical calculations suggest that Cc_{550} could also contribute to entry/exit channels for water or protons from the Mn_4CaO_5 cluster (Umena et al. 2011; Vogt et al. 2015), although the role of Cc_{550} has been recently put in discussion (Takaoka et al. 2016). Beyond a structural function, a redox role of the cytochrome heme cofactor in PSII has not been established. In addition, in many organisms Cc_{550} can be mostly purified as a soluble protein (Evans and Krogmann 1983; Navarro et al. 1995; Kerfeld and Krogmann, 1998). Thus, it would be possible that two different populations of Cc_{550} are present: one bound to the PSII and the second one soluble in the lumen (Kirilovsky et al. 2004). Several roles for this soluble Cc_{550} have been proposed in cyanobacteria, mostly in anaerobic carbon and hydrogen metabolism (Krogmann 1991; Morand et al. 1994; Kang et al. 1994), cyclic photophosphorylation (Kienzel and Peschek 1983) and in the reduction of nitrate to ammonia (Alam et al. 1984).

Cyanobacterial Cc_{550} shows intriguing structural and biophysical properties. In addition to the unusual bis-histidinyl axial heme coordination, the protein has a very low midpoint redox potential (E_m) when purified as the soluble form (from –250 to –314 mV) (Alam et al. 1984; Navarro et al. 1995; Roncel et al. 2003), but much more positive potential values were obtained for the Cc_{550} bound to PSII (from –80 to +200 mV) (Roncel et al. 2003; Guerrero et al. 2011). On the other hand, the EPR spectra of the different cyanobacterial Cc_{550} studied in the oxidized form are typical of a low-spin heme with bis-

histidine coordination (Roncel et al. 2003; Kerfeld et al. 2003). Finally, minor, but significant differences in the EPR spectra from the free and PSII-bound Cc_{550} were observed (Roncel et al. 2003; Kirilovsky et al. 2004).

Diatoms belong to the red lineage of algae that diverged along evolution from the green lineage that evolved to higher plants (Bowler et al. 2008; Grouneva et al. 2013) and nowadays constitute the most abundant and diversified group of oceanic eukaryotic phytoplankton (Kooistra et al. 2007; Bowler et al. 2010). The photosynthetic chain in diatoms possesses some peculiarities, arising from their double endosymbiotic origin. Thus, the assembly of extrinsic proteins at the lumenal side of PSII includes the three cyanobacterial-like subunits PsbO, PsbU and PsbV (or Cc_{550}), as well as the PsbQ' subunit also present in red algae (Enami et al. 1998; Nagao et al. 2007, 2010a,b). However, besides these subunits, diatoms have an extra extrinsic protein, named as Psb31 (Okumura et al. 2008). Reconstitution experiments of isolated PSII samples depleted of the extrinsic subunits indicate that both in red and diatoms algae the binding of PsbV/Cc_{550} requires prior binding of PsbO and PsbQ' and, in the case of diatoms, of Psb31 (Enami et al. 1998, 2003; Nagao et al. 2010b). This contrasts with the results obtained in cyanobacteria, where Cc_{550} is able to bind directly to the PSII core complex in a manner essentially independent of other extrinsic subunits (Enami et al. 2003), although PsbO is also required for a functional binding of Cc_{550}, as revealed both by reconstitution and Fourier transform infrared spectroscopy experiments (Shen and Inoue 1993; Nagao et al. 2015). It is interesting, however, to note that the very recent crystal structure of the PSII from the red alga *Cyanidium caldarium* has shown an overall structure similar to the cyanobacterial complex, including the position of Cc_{550} in PSII (Ago et al. 2016).

In this work, we have purified and characterized the Cc_{550} from the diatom *Phaeodactylum tricornutum*. The protein is obtained in a C-terminal truncated form with a low affinity for the PSII complex. In addition, the characterization of *Phaeodactylum* Cc_{550} by continuous wave and pulse EPR indicates a relationship between the electrostatic environment of the heme centre within the protein heme-pocket and the electronic structure of the paramagnetic entity.

EXPERIMENTAL PROCEDURES

Cell cultures

Cells from the coastal diatom *Phaeodactylum tricornutum* CCAP 1055/1 (hereafter *Phaeodactylum*) were used as biological material. *Phaeodactylum* cells from photobioreactors outdoor cultures were obtained as a frozen paste from Easy Algae (Cádiz, Spain). Alternatively, *Phaeodactylum* was grown in Artificial Seawater (ASW) medium (McLachlan 1964; Goldman and McCarthy 1978) in a rotatory shaker (50 rpm) at 20 ºC. The cultures were illuminated by fluorescent white lamps giving an intensity of 20 µE m^{-2} s^{-1} under a light/dark cycle of 16/8 h. For the experiments of the effects of iron deficiency, cells from cultures of 15 days were pelleted at 5,000x*g* for 5 min and grown in standard ASW medium (iron-replete culture; 12 µM Fe) and ASW medium with only 0.12 µM Fe (iron-deplete culture), with regular transfer of the cells into fresh media. In the experiments of Cc_{550} and cytochrome c_6 (Cc_6) quantification after changing iron availability, cultures grown under iron-replete or iron-deficiency were divided in two equal volumes, centrifuged (5,000x*g* for 5 min) and resuspended in the same volume of iron-replete or iron-deficient media. Four sets of samples were thus obtained: (1) cells growing in iron-replete medium and (2) cells growing in iron-deficient medium, resuspended in their same fresh medium; (3) cells growing in iron-deficient medium resuspended in fresh iron-replete medium; and (4) cells growing in iron-replete medium resuspended in fresh iron-deficient medium.

Proteins purification

Purification of Cc_{550} from *Phaeodactylum* cells was carried out as a modification of the procedure recently described for the purification of Cc_6 from the same organism (Navarro et al. 2011; Bernal-Bayard et al. 2013). The method consisted of cell resuspension in 10 mM MES, pH 6.5, 2 mM KCl and 5 mM EDTA buffer, supplemented with DNase and the protease inhibitors PMSF, benzamidine, aminocaproic acid and a tablet of the cOmplete Protease Inhibitor Cocktail (Roche), followed by French press disruption (20,000 psi), treatment with streptomycin sulfate, sequential precipitation with 30 and 60 % ammonium sulfate and extensive dialysis, to obtain the clarified crude extract. From this point Cc_{550} was purified by FPLC, first by using a DEAE Sepharose column (Cc_{550} elution by applying a 0.01–0.2 M NaCl linear gradient in Tris-HCl 10 mM, pH 7.5 buffer) and further by gel filtration using a Sephacryl S-200 HR column (GE Healthcare Life Sciences). Protein fractions with an A_{550}/A_{275} ratio close to 1.0 were pooled, suspended in Tris-HCl 10 mM, pH

7.5 buffer, concentrated in an Amicon pressure filtration cell, and finally frozen at –80 ºC until use. The concentration of Cc_{550} was calculated using an extinction coefficient of 26 mM^{-1} cm^{-1} at 550 nm for the reduced form (Shimazaki et al. 1978; Navarro et al. 1995).

PSII-enriched samples from *Phaeodactylum* cells were obtained by ß-dodecyl-maltoside (ß-DM) solubilization and sucrose gradient separation. Fresh *Phaeodactylum* cells were resuspended in 50 mM MES, pH 6.5, 5 mM $MgCl_2$ and 5 mM EDTA buffer (buffer A), supplemented with proteases inhibitors and 1 M betaine or sorbitol (buffer B), and disrupted in a French pressure cell at 7,000 psi. Some control experiments were carried out with cells resupended in buffer A (non-osmotically stabilized buffer) and disrupted by 6 cycles of freezing in liquid nitrogen and thawing at 25 °C in a thermoblock. In any case, unbroken cells were separated by centrifugation at 5,000x*g* for 5 min and the supernatant (crude extract) was centrifuged at 170,000x*g* for 30 min. The resultant supernatant was considered as the soluble fraction, whereas the pellets were resuspended in buffer B and centrifuged as before to obtain a washed fraction (the supernatant) and a thylakoids extract (the pellets). Pellets were resuspended in buffer A supplemented with 0.2 M sucrose at 1 mg Chl mL^{-1} and later diluted to 0.5 mg Chl mL^{-1} with the same volume of ß-DM 3% (w/v), prepared in buffer A, to yield a final detergent:chlorophyll ratio of 30:1 (w/w), and the solution was incubated 30 min in the dark at 4 ºC under gentle stirring. Control experiments were carried out using a mixture of 0.5 mg Chl mL^{-1} and ß-DM 0.5% (final detergent:chlorophyll ratio of 10:1), followed by incubation at 4 ºC for 5 min. Finally, solubilized solutions were centrifuged at 170,000x*g* for 30 min and the resulting supernatant (detergent-solubilized fraction) was loaded onto a continuous sucrose density gradient from 0.17 to 0.47 M sucrose, prepared in buffer A + 0.03% ß-DM, and centrifuged at 135,000x*g* for 16 h. The medium mostly-green band was collected and considered as a PSII-enriched sample. The PSII content was calculated from the differential (ascorbate minus ferricyanide) absorbance change of the PSII-intrinsic cytochrome b_{559} protein (Roncel et al. 2003). The content of Cc_{550} was estimated from the absorbance difference at 550 nm between the reduced (sodium dithionite, 1 mM) and oxidized state (in the presence of sodium ascorbate 1 mM), using a differential extinction coefficient (reduced minus oxidized) of 15 mM^{-1} cm^{-1} at 550 nm (Navarro et al. 1995).

Analytical methods

The N-terminus of purified Cc_{550} was sequenced in a Procise TM 494 Protein Sequencer (Applied Biosystems) at the *Protein Chemistry Service* (CIB-CSIC, Spain). Redox titrations

were performed as described previously (Molina-Heredia et al. 1998; Guerrero et al. 2014) in potassium phosphate 50 mM (pH 7) or acetic-acid/MES (25:25 mM, pH 5-6) buffers, in the presence of 10 μM of anthraquinone-2-sulfonate, 2-hydroxy-1,4-naphthoquinone and duroquinone as redox mediators. The accuracy of the potential-measuring system was first tested by redox titration of a flavin-mononucleotide solution as a standard ($E_{m,7}$ = –220 mV). Chlorophyll concentrations were determined as previously reported (Arnon 1949; Jeffrey and Humphrey 1975).

The total Cc_{550} content in *Phaeodactylum* cells was determined by differential absorbance measurements. 40-100 mL cultures were precipitated by centrifugation at 16,000x*g* for 5 min and wet pellets were weighed. Cells were then resuspended to 1 mL in culture media and frozen until use. Unfrozen samples were disrupted by 6-7 cycles of freezing in liquid nitrogen and thawing at 30 °C in a thermoblock. Soluble fractions were obtained by centrifugation at 16,000x*g* for 15 min, and the content of Cc_{550} was estimated as before. This method extracted up to 85-90% of Cc_{550}, as determined by further protein extraction by sonication of the membrane fractions. Control measurements of the Cc_6 content were made from the absorbance difference at 552 nm between the fully reduced (sodium ascorbate, 1 mM) and fully oxidized (potassium ferricyanide, 0.5 mM) states (Roncel et al. 2016). The amount of Cc_{550} or Cc_6 was related to grams of the initial wet weight. Some additional experiments were designed to estimate the amount of soluble (or easily removed from membranes) and membrane-associated Cc_{550} (and Cc_6). Briefly, *Phaeodactylum* cells were resuspended in 50 mM MES, pH 6.5, buffer supplemented with 10 mM $MgCl_2$, 1 M betaine, proteases inhibitors and DNase, and disrupted by a French press cycle at 7,000 psi. Unbroken cells were separated by centrifugation at 5,000x*g* for 5 min and the supernatant was centrifuged at 170,000x*g* for 25 min. The resultant supernatant was considered as the soluble fraction, whereas the pellet was resuspended in the same buffer and centrifuged as before to obtain a washed fraction (the supernatant) and a membrane extract (the pellet). Cc_{550} was extracted from this membrane fraction by resuspension in 50 mM MES buffer, pH 6.5, supplemented with 500 mM NaCl and 4 % Triton X-100 detergent, followed by 30 min incubation in the dark. Solubilized proteins were separated by centrifugation (170,000x*g* for 25 min) and partially purified by sequential precipitation with 50 and 85 % ammonium sulfate. The final pellet (membrane associated fraction) was resuspended in few mL of potassium phosphate 50 mM, pH 7, buffer, and the amounts of Cc_{550} (and Cc_6) were estimated as before. Alternatively, the final pellet was resuspended in

pure water, washed by two dilution/concentration cycles in an Amicon pressure filtration cell, and used for molecular weight MALDI-TOF analysis.

For the immunodetection of Cc_{550}, polyclonal antibodies raised against this cytochrome were generated using standard procedures at the *Animal Experimentation Facility* (University of Seville, Spain) by subcutaneous injection of 1 mg of purified protein into a white New Zealand rabbit (Bernal-Bayard et al. 2013). Antibodies against D1, PsbO (Agrisera, Sweden) and Psb31 from the diatom *Chaetoceros gracilis* (a generous gift of Prof. T. Tomo, Tokyo University of Science, Japan) were also used. Protein samples or cell extracts were resolved on 15% (w/v) polyacrylamide gel electrophoresis and transferred to a nitrocellulose membrane (Amersham Protran Premium 0.45 µm NC, GE Healthcare Life Sciences). The membrane was incubated overnight with the primary antibodies (dilution 1:1,000) followed by 1 h incubation with Goat Anti-Rabbit IgG (H+L)-HRP Conjugate (Biorad) (dilution 1:10,000), and visualized with the Immobilon Western Chemiluminescent HRP Substrate (Millipore). Western blot bands were quantified using the Quantity One® 1-D analysis software (Bio-Rad).

Matrix-Assisted Laser Desorption/Ionization Time-of-Flight Mass Spectrometry (MALDI-TOF MS)

MALDI-TOF MS analyses were performed at the *Proteomic Service* (IBVF, Sevilla, Spain), in an Autoflex model analyzer (Bruker Daltonics, Germany) operated in lineal (protein molecular weight) or reflector (peptide mass fingerprint) positive modes. Mass spectra were previously calibrated with appropriate standards to the range of mass under study. The molecular weight (MW) of Cc_{550} was determined with sinapinic acid as matrix, whereas HCCA (α-cyano-4-hydroxy-cinnamic acid) was used as the matrix for peptide mass fingerprint. Tryptic digestion and BrCN cleavage were carried out as described elsewhere (Sechi and Chait 1998; Crimmins et al. 2005; Martínez-Fábregas et al. 2014) and the peptide fingerprint was obtained by MALDI-TOF MS. Protein identification was carried out by comparing the obtained peptide fingerprint with the NCBI database using the MASCOT software programs.

Electron paramagnetic resonance (EPR) spectra

Protein samples for EPR were prepared in Tris-HCl 10 mM, pH 7.5 buffer, supplemented with glycerol in a 2:1 ratio, to obtain a glass upon freezing. Subsequently, samples were

transferred to 4 mm quartz EPR tubes, frozen in liquid nitrogen and stored until use. The resulting protein concentration was 0.6 mM.

Both, continuous wave (CW) and pulse EPR measurements were performed on a Bruker Elexsys spectrometer (Bruker Biospin, Germany) operating at X-Band (about 9.6 GHz), either equipped with a rectangular cavity operating in the TE102 mode or a DM5 dielectric ring resonator, for CW and pulse measurements respectively. The experiments were performed at very low temperatures by means of a helium gas-flow cryostat and a temperature controller, both from Oxford Instruments (UK).

The CW-EPR spectra were taken at 25 K adjusting the microwave power to ensure that there was no saturation. Modulation frequency and amplitude of the magnetic field were 100 Hz and 1 mT respectively. All pulse EPR experiments were recorded between 6 and 8.5 K and a shot repetition time of 2 ms. Electron Spin Echo detected field-sweep spectra were recorded with the Hahn-echo sequence $\pi/2$ - τ - π. 2D Hyperfine Sublevel Correlation experiments (HYSCORE) were performed using the standard sequence $\pi/2$ - τ -$\pi/2$ - T1 - π - T2 -$\pi/2$ with an eight-step phase cycle (Schweiger and Jeschke 2001).

Processing of the 2D HYSCORE spectra included a polynomial baseline correction, hamming windowing in both dimensions before performing a 2D Fast Fourier Transform. The absolute value of this transform was displayed in the 2D frequency domain.

Structural model

The structure of Cc_{550} from *Phaeodactylum* was modeled using the program Phyre[2] (http://www.sbg.bio.ic.ac.uk/phyre2/html/) (Kelly and Sternberg 2009), employing as main templates the crystal structures of Cc_{550} from *Thermosynechococcus elongatus* (pdb 1MZ4 and 1W5C) and *Synechocystis* sp. PCC 6803 (pdb 1E29). Surface electrostatic potentials were calculated and represented using the Swiss-Pdb Viewer Program (Guex and Peitsch 1997).

RESULTS

Protein purification and analytical characterization

Figure 1 shows the different purification and protein extraction procedures carried out during the characterization of Cc_{550} from the marine diatom *P. tricornutum*. First, by following a modification of previously described purification methods (see the Experimental Procedures section), a yield of ca. 15 mg of purified Cc_{550} was obtained from 100 g wet weight of *Phaeodactylum* cells, from about 30 mg present in the initial supernatant after the streptomycin sulfate treatment, as determined by the differential absorbance changes (not shown). The Cc_{550} obtained in the soluble fraction was about 85% of the total (*i.e.*, 35 mg), as also estimated from differential absorbance changes. Thus, *Phaeodactylum* cells disruption at high pressure in a non-osmotically stabilized medium allowed to extract moderately large amounts of solubilized Cc_{550}. Visible absorption spectra of purified Cc_{550}, both in the native oxidized and dithionite-reduced forms, show absorption bands (549.5, 521 and 417 nm, reduced; 405.5 and 528.5 nm, oxidized) similar to those previously described (Shimazaki et al. 1978; Navarro et al. 1995) (Figure S1, supplementary material). The absorbance ratio A_{275} (oxidized)/A_{550} (reduced) for the final purest protein samples was 1.07. Redox titration of *Phaeodactylum* Cc_{550} established a midpoint redox potential ($E_{m,7}$) value of –190±12 mV (Figure S1, supplementary section) which did not significantly change in the pH range 5-7 (data not shown). This potential value, although maintaining the typical negative redox potential, is significantly more positive than those described in cyanobacteria for Cc_{550} in solution (–250 to –300 mV) (Navarro et al. 1995; Roncel et al. 2003; Guerrero et al. 2011).

Interestingly, when checking the MW of purified Cc_{550} by MALDI-TOF analysis, a value of ca. 15,110 Da was obtained (Figure 2A). After subtracting the heme group (616 Da), a MW of ca. 14,495 for the peptide chain is consequently deduced. This value is lower than the theoretical value inferred from the *psbV* gene sequence (ca. 14,822 for the peptide chain and 15,438 for the heme-containing holoprotein; see Figure 2) but agrees with a truncated protein in the two last tyrosine residues of the C-terminus (14,495.5 for the peptide chain and ca. 15,111 for the holoprotein; Figure 2). Actually, no signal corresponding to the theoretical sequence has been detected in any case (see below), although an even smaller band of much lower intensity was also identified, whose MW (14,997.6 Da) could fit with an additional small fraction of a truncated protein in the last three residues of the C-terminus (14,998.4 for the peptide chain; Figure 2A).

Different experiments were carried out to confirm the occurrence of a C-terminal truncated protein. First, the N-terminal part of purified Cc_{550} was sequenced (data not shown), showing the correct sequence according to the *psbV* gene (IDLDEATRTV; Figure 2, *lower*). Second, Cc_{550} samples were subjected to trypsin or BrCN cleavage and peptide analysis (Figure S2, supplementary material). Trypsin digestion unequivocally identified the sample as the Cc_{550} protein, without the observation of additional peptides arising from alternative proteins (data not shown). However, lysines 129 and 134 in Cc_{550} (targets for trypsin) prevented the possible identification of the last protein C-terminus part when using this protease, and thus BrCN was alternatively used. As shown in Figure S2 (supplementary material), BrCN cleavage allowed the identification of peptides covering residues 1-115, but the expected peptide corresponding to the 116-137 residues in the C-terminus (MW=2,471.9 Da) was absent. Conversely, new peptides compatible with the lack of the 2-3 C-terminus groups appear (Figure S2), thus confirming the occurrence of truncated species. It is also important to note that the truncated Cc_{550} not only appears in the final purified protein, but also in the initial clarified crude extract from the purification process (MW ≈ 15,107; Figure 2B), although in this case the data are less accurate due to the lower protein concentration and to interferences arising from other cellular components.

In order to better establish the Cc_{550} distribution and nature (truncated or not) between soluble (or easily membrane-released) and membrane-associated fractions, *Phaeodactylum* cells were disrupted in osmotically stabilized media (in the presence of betaine or sorbitol) under a lower pressure (7,000 psi) and Cc_{550} was quantified by the differential absorbance changes, both in the soluble fraction and in the fraction extracted from membrane samples treated with 500 mM NaCl and 4% Triton X-100 (Figure 1). As an additional control, the soluble luminal Cc_6 protein was also quantified in the different samples. From the differential absorbance spectra (reduced *minus* oxidized) corresponding to Cc_{550} and Cc_6 in samples obtained after treating the membrane fractions with NaCl and detergent (Figure S3, supplementary material), it was possible to estimate that the membrane-associated proteins stand for ≈ 40% and 10% of total Cc_{550} and Cc_6, respectively (60% and 90% in the soluble protein fraction), no differences being observed when using betaine or sorbitol as osmotic stabilizing agents (data not shown). The presence of a small amount of Cc_6 in the membrane-extracted fraction, as well as the fact that washing the membranes with the disruption buffer, instead the salt/detergent mixture, did not result in a significant extraction of either Cc_{550} or Cc_6 (not shown), indicate that at least a part of the membrane-extracted Cc_{550} would arise from disruption of closed thylakoids during the

detergent washing procedure. To test if the soluble and the membrane-associated Cc_{550} correspond to different forms (*i.e.*, a soluble but truncated protein, and a membrane-bound and complete protein) a MW MALDI-TOF analysis of Cc_{550} partially purified from the membrane-extracted fraction was carried out. The results indicated again a truncated protein, similar (MW ≈ 15,106) to that obtained in the soluble fraction, without any detection of the theoretical complete protein (Figure 2C).

The affinity and association of Cc_{550} to PSII has been investigated by Western blot analysis of the different fractions acquired along the obtainment of PSII-enriched samples from *Phaeodactylum* by ß-DM solubilization (Figure 1), a standard method used for PSII purification (Enami et al. 1995; Bumba et al. 2004; Kirilovsky et al. 2004; Nagao et al. 2007). Cc_{550} and both the D1 core and the extrinsic PsbO and Psb31 subunits of PSII were monitored. Psb31 is exclusive of diatoms, and its presence along PSII purification is particularly relevant as it has been described to be required for the binding of Cc_{550} to the photosystem complex (Okumura et al. 2008; Nagao et al. 2010a). Additionally, direct spectroscopic monitoring of the PSII core (the cytochrome b_{559}) and Cc_{550} in the different fractions from the sucrose gradient was also carried out. From the immunological analysis shown in Figure 3 it is first confirmed that although Cc_{550} appears in the soluble fraction, a significant amount of the protein can be also observed both in the initial and washed membrane fractions, as well as in the ß-DM solubilized sample, together with the D1, PsbO and Psb31 subunits (Figure 3, *upper*). However, after sucrose gradient partitioning, Cc_{550} is located mostly in the top low-density fraction, corresponding to free (not-associated to PSII) Cc_{550} (Figure 3, *upper*), whereas D1 and Psb31 only appear in the high-density lower green band containing PSII, and PsbO is significantly located in both fractions. The quantification of the Western blot bands resulted in an amount of Cc_{550} and PsbO in the PSII fraction of ca. 10% and 34%, respectively (90% and 66% in the top soluble fraction). The low content of Cc_{550} in the PSII-enriched samples was also confirmed by spectroscopic measurements of the differential absorbance changes associated both to this protein and cytochrome b_{559}. Thus, whereas cytochrome b_{559} was clearly monitored, only minor changes at 562 nm (probably associated with the cytochrome b_6f complex) were observed under dithionite reduction, and no significant changes associated to Cc_{550} were detected (Figure 3, *lower*). However, Cc_{550} was clearly identified in the upper gradient fraction (Figure 3, *lower*). Similar results were obtained using a lower detergent:chlorophyll solubilization ratio and time (1:10 and 5 min; see the Experimental Procedures section), although in this case a lower PSII purification yield was observed (not shown).

It is well known that iron availability limits growth of photosynthetic algae and of diatoms in particular (Allen et al. 2008; Morrissey and Bowler 2012; Nunn et al. 2013). A down-regulation under iron limitation of several iron-containing proteins has been previously reported in *Phaeodactylum*, although the global PSII concentration and D1 transcription is maintained, and other PSII subunits, including Cc_{550}, were described to remain almost constant (Allen et al. 2008). Recently we have reported a decrease to a level of ca. 30% of the Cc_6 protein content in iron-deplete cells as compared with iron-replete conditions (Roncel et al. 2016). Considering that at the protein level the amount of both Cc_6 and Cc_{550} is similar in *Phaeodactylum* cells (this work, and see Bernal-Bayard et al. 2013; Roncel et al. 2016), we have here investigated the evolution of the Cc_{550} content when changing iron availability. It is interesting first to note that cultures grown under low iron availability showed levels of Cc_6 and Cc_{550} of 25-30% and 45-50%, respectively, compared with iron-replete conditions, as estimated by its specific redox differential absorbance changes (Figure 4A,C). Thus, from these values it seems that down-regulation under low iron of the electron donor to PSI (the Cc_6) is higher than the PSII-associated Cc_{550} protein. In addition, cultures grown under iron-replete or iron-limiting conditions were collected and resuspended in the same volume of iron-deplete or iron-replete media, respectively, and the content in Cc_{550} and Cc_6 was followed during several days of culture. As shown in Figure 4B, when shifting from replete to deplete (+/–) or from deplete to replete (–/+) conditions, a decrease or a parallel increase in the content of Cc_{550}, respectively, were observed, these changes occurring during the first 6 days of culture. Similar qualitative results were obtained when analyzing the Cc_6 content (Figure 4D).

EPR measurements

The CW-EPR spectrum of the soluble form of *Phaeodactylum* Cc_{550} is presented in Figure 5A, where it shows the three characteristic features of a low-spin heme ($S = ½$), with g factor absolute values of $|g_z| = 3.00$, $|g_y| = 2.24$ and a broad signal at high field centered at $|g_x| = 1.44$ (Table 1). The electron spin echo (ESE) detected EPR spectrum, normally much more sensitive to broad signals since it is displayed in the absorption mode, confirms the g values (Figure 5B). EPR spectra of low-spin heme centers are usually analyzed with the *hole-model* (Griffith 1957; Taylor 1977). Using this model it is possible to obtain the relative energy levels of the t_{2g} orbitals of the iron atom, where the unpaired electron is distributed (Alonso et al. 2007; Alonso and Martínez 2015). The level distribution can be parametrized by the

crystal field parameters Δ and V (Figure 5C), which can be calculated in units of the spin-orbit coupling constant, λ, from the *g*-values. In our case, the estimated values (Table 1) were: Δ/λ = 3.17, V/λ = 1.71, and subsequently V/Δ = 0.54. These parameters are typical for a bis-histidine coordination (Peisach et al. 1973, and see Table 1). HYSCORE experiments were undertaken in this variant to study the hyperfine interaction of the electron spin in the iron with the nuclear spin (I =1) of the coordinating nitrogens (Figure 5D). The experiments were performed at the magnetic field corresponding to g_z (B = 230 mT), where the magnetic field is perpendicular to the heme plane. In the negative quadrant of the experiment, it can be observed the so-called double-quantum (dq) correlation peaks (Figure 5D), which are the ones normally more intense in HYSCORE spectra of low-spin hemeproteins (García-Rubio et al. 2003; Ioanitescu et al. 2007). In this case, and unlike other proteins and low-spin heme model complexes where one peak for heme and one peak for histidine are observed at this position, up to four such peaks are solved. The assignment of these peaks to particular nitrogens is difficult, due to the low sensitivity in the single-quantum region at lower frequencies. Irrespectively of the particular assignment of peaks in the spectrum to coordinated nitrogen atoms, there is certainly a lack of equivalency in the hyperfine coupling of the heme nitrogens, since at least two of the peaks have to be assigned to heme nuclei (there are four peaks and four heme nitrogens and two histidine nitrogen nuclei). Similar inequivalencies of heme nitrogens in HYSCORE spectra have already been reported in other hemeproteins (Van Doorslaer et al. 2012).

DISCUSSION

Cc_{550} is an extrinsic component in the luminal side of PSII in cyanobacteria, but also in eukaryotic algae from the red photosynthetic branch, which comprises diatoms (Enami et al. 2008; Roncel et al. 2012). We have here characterized the Cc_{550} from the model diatom *Phaeodactylum tricornutum*, in order to shed light on the different evolutionary pathways of PSII in the different branches of photosynthetic organisms. Is is interesting to note that although a Cc_{550}-like protein (encoded by the *psbV2* gene) has been identified in several cyanobacteria (Kerfeld et al. 2003; Suga et al. 2013), *Phaeodactylum* only possesses the canonical Cc_{550} protein, encoded by the chloroplast *psbV* gene.

Cc_{550} can be obtained from the soluble cell extract in relatively large amounts. An $E_{m,7}$ value of ca. –190 mV was estimated for the purified protein. This value is at least 60 mV more positive than values described in cyanobacteria at pH 7 for the protein in solution (Navarro et al. 1995; Roncel et al. 2003; Guerrero et al. 2011). Although in *T. elongatus* the redox potential is pH-dependent and varies from –150 to –350 mV as the pH increases from 5 to 10 (Roncel et al. 2003), in *Phaeodactylum* the redox potential remains basically constant in the pH range from 5 to 7. Remarkably, more positive but pH-independent redox potential values (varying from –80 to +200 mV) have been obtained for the Cc_{550} bound to PSII (Roncel et al. 2003; Guerrero et al. 2011). However, because the very weak binding (see below), it was not possible to measure the redox potential of the PSII-bound Cc_{550} in *Phaeodactylum*.

It is interesting to compare the Cc_{550} content in *Phaeodactylum* cells (ca. 35 mg from 100 g of wet weight) with the lumenal (and soluble) Cc_6 (ca. 25 mg in the same cell amount), which corresponds to a molar ratio Cc_6/Cc_{550} ratio of ≈1.15. It has been previously reported that the Cc_6 concentration in the thylakoid lumen would be as high as ca. 200 μM (Haehnel et al. 1989; Durán et al. 2005), which is in agreement with our protein content measurements in *Phaeodactylum* cells. Thus, according to this comparison, a tentative concentration of Cc_{550} in the lumen of ca. 175 μM could be estimated.

Phaeodactylum Cc_{550} is purified in a truncated form, lacking the last two C-terminal tyrosines, as clearly demonstrated by MS analysis (Figure 2), although a much smaller population of a truncated form lacking the last three C-terminal residues cannot be discarded. Thus the question arises about the physiological relevance of this fact, *i.e.*, if the truncated Cc_{550} is the result of a specific processing or to the unspecific exposition of the protein to cell proteases during the purification course. Although the occurrence of an

artifactual protein truncation cannot be totally rejected, several facts speak in favor of a physiological process. First, the purification procedure has been carried out in the presence of a wide battery of proteases inhibitors. Second, in spite of the relatively high amount of Cc_{550} present in the initial crude extracts (see above), no traces of the theoretical complete protein have been detected in any case during the different steps of purification. Finally, the analysis of Cc_{550} extracted from membrane fractions also points to a physiological truncated protein form. The procedure followed in these latter experiments (lower pressure disruption, membranes washing and detergent extraction) yielded a substantial membrane-bound Cc_{550} population, even partially arising from a small but significant thylakoid fraction enclosing the protein, as deduced by the presence of detectable amounts of the luminal soluble Cc_6. A membrane-extracted Cc_{550} should not have been in contact with other proteases than those from the chloroplast, since the Cc_{550} bound to PSII would have its C-terminus not accessible to proteases, as deduced by the known PSII crystal structures of cyanobacteria and red algae (Shen 2015; Ago et al. 2016, and see below). It is interesting to note that in the diatom *Thalassiosira oceanica*, in addition to the canonical Cc_{550} gene with a KIYF C-terminus sequence, an additional Cc_{550}-like gene (ca. 97 % identity) corresponding to a protein with a truncated C-terminus sequence, lacking the three last hydrophobic residues, has been reported (THAOC_28383 gene).

If the processing of Cc_{550} is a specific physiologically relevant event, it could occur either at the RNA or the protein level, in this latter case probably associated to a carboxypeptidase activity. Several serine and zinc carboxypeptidases are annotated in the *Phaeodactylum* genome, although a chloroplast location is not established (Bowler et al. 2008). Thylakoid proteolytic activities are mainly associated to PSII turnover, related to photochemical oxidative effects and to dynamic adaptations under different environmental conditions (Aro et al. 1993; Kato and Sakamoto 2010). An enhanced PSII turnover has been suggested in diatoms (Key et al. 2010; Wu et al. 2011; Nagao et al. 2013, 2016; Lavaud et al. 2016), and in *C. gracilis*, in particular, the PSII complex was described to be remarkably unstable and rapid protein degradation was observed (Nagao et al. 2007, 2012). In addition, at least four new proteases were detected in the thylakoid membranes of this diatom (Nagao et al. 2012). It is interesting to note that from the first crystal structure of soluble Cc_{550} from the cyanobacterium *Synechocystis* sp. PCC 6803, it was initially suggested that residues of the C-terminal form a hydrophobic finger maybe involved in the interaction with PSII (Figure 6) (Frazao et al. 2001). This proposal has been later confirmed in the structure of PSII from the cyanobacterium *T. elongatus* (Shen 2015) and, very recently, in the PSII

structure from the red alga *C. caldarium* (Ago et al. 2016). Furthermore, in *T. elongatus* the last residues in the C-terminus of the Cc_{550} are not resolved in the soluble structure but are visible in the crystal structure, when Cc_{550} is bound to PSII (Kerfeld et al. 2003). This indicates that this region is much more flexible when the cytochrome is in its soluble form, pointing to a direct role in binding to PSII, where this region of the protein is structured. Thus it is possible to speculate that a truncated protein in its C-terminus could have a diminished affinity for the PSII complex and thus a facilitated release during PSII turnover. The modelled structure of *Phaeodactylum* Cc_{550} displays a general folding very similar to that described in other cyanobacterial and red algae Cc_{550} (Figure 6), and thus the complete diatom protein shows the hydrophobic protuberance pointing up –according the orientation presented in Figure 6–, although this protuberance is sensibly diminished in the truncated Cc_{550} form. Interestingly, the electrostatic surface of the diatom cytochrome also shows a distinctive character, as the protein exhibits a diminished negatively charged surface (Figure 6). This fact would be also relevant in setting the affinity binding to PSII.

From the *g*-values obtained from the EPR spectra, it is possible to calculate the crystal field parameters Δ/λ and V/λ and reconstruct the energy levels of the t_{2g} orbitals (Alonso et al. 2007). There have been quite a lot of very informative studies on bis-imidazole model complexes to determine how the geometry of the axial ligands can affect this energy diagram, interpreting it in terms of π donation, steric hindrance or other kinds of interactions (Walker et al. 1986; Quinn et al. 1987). In such studies, the crystal field parameters, and especially V, are linked with the dihedral angle between histidines (Walker et al. 1986) and the angle between the imidazole planes and the axis N_p – Fe – N_p (Quinn et al. 1987). Based on these studies on heme model complexes, the parameter V/Δ for the cyanobacterial *T. elongatus, Synechocystis* 6803 and *Arthrospira maxima* Cc_{550} hemes was related to a figure accounting for the "global distortion" of the axial ligands, quantified as the sum of a total of eight angles obtained from the three crystalline structures known at the time of this study (Kerfeld et al. 2003). According to this analysis, an important further distortion of the axial ligands upon binding of Cc_{550} to PSII should be expected. However, the structures of PSII from the cyanobacterium *T. elongatus* and the red alga *C. caldarium* (Loll et al. 2005; Ago et al. 2016) show only a very minor rotation of the heme upon binding, as compared with soluble Cc_{550}. Moreover, changes in the geometry of the axial ligands among the different soluble variants are also very moderate, and they do not correspond with the results of Quinn et al. (1987), where a decrease in V/Δ from 0.62 to 0.54

corresponds to a rotation of both imidazole planes of around 20 degrees. Therefore, the observed differences in *g*-values among the different soluble Cc_{550} variants cannot, or at least not entirely, be due to the very minor observed differences in the axial ligand geometry (Frazao et al. 2001; Kerfeld et al. 2003).

The *g*-values are also known to be very sensitive to changes in the electrostatic environment of the paramagnetic center and, related to it, to hydrophobicity changes (Yruela et al. 2003). Although the backbone structure is highly conserved among different Cc_{550} proteins, important differences in polarity and surface charge distribution exist (Figure 7). Note that non-conserved residues close to both His67 and His118 axial ligands (*i.e.* A65Q, G69Q, I114Y and A115S in the alignment shown in Figure S4, supplementary data) change the polarity in the heme pocket of *Synechocystis* Cc_{550} respect to *T. elongatus*, which is much closer to *Phaeodactylum* (Figure 7). The variations observed in the *g*-values and related crystal-field parameters (Table 1) could be associated to these polarity changes. Considering that binding to PSII will probably involve electrostatic and hydrophobic interactions not far away from the heme (Guerrero et al. 2011; Shen 2015; Ago et al. 2016), it could be responsible for the changes observed in *g*-values between soluble and PSII-bound Cc_{550} variants. In turn, changes in solvent accessibility produced upon binding most likely account for the change in the redox potential (Guerrero et al. 2011).

The effect of the environment on the heme center is also observed from the HYSCORE measurements. In heme model compounds, the symmetry of the paramagnetic entity is preserved in such a way that molecular, electronic and magnetic axes keep a well-defined relationship. Particularly, a Z-axis perpendicular to the heme plane is common to these three frames (García-Rubio et al. 2003; Alonso et al. 2007). As a consequence, HYSCORE spectra of these model systems in the g_z position show only two dq peaks, provided that the two hyperfine splittings of the axial nitrogen nuclei are equivalent, as well as those of the four porphyrin nitrogen nuclei. On the other hand, when the symmetry of the paramagnetic entity environment is broken, as in the heme center within some proteins, the relationship between molecular and magnetic axes disappears (Alonso et al. 2007). Then inequivalence between nitrogen hyperfine splittings can be detected in HYSCORE spectra, as it is here shown in Figure 5D.

PSII is a labile complex, and the lack of luminal extrinsic subunits, including Cc_{550}, is not unusual during purification experiments (Martinson et al. 1998; Nagao et al. 2007; Grouneva et al. 2011). This could be particularly true in *Phaeodactylum*, as this diatom is not disrupted by freeze/thawing cycles in an osmotically stabilized buffer, and pressure

disruption is thus required. This contrasts with PSII purification in the diatom *C. gracilis*, for which freeze/thawing disruption allowed to obtain PSII particles containing most of the extrinsic luminal subunits by column chromatography (Nagao et al. 2007). These studies determined that diatoms have an extra extrinsic protein, Psb31, in addition to the other four subunits also present in red algae: PsbO, PsbU, PsbQ' and PsbV (Enami et al. 1998; Okumura et al. 2008; Nagao et al. 2010a). Reconstitution experiments of PSII samples have suggested that both in red algae and diatoms the binding of PsbV (and PsbU) requires previous PsbO and PsbQ' binding and, in the case of diatoms, also the binding of Psb31, the last three proteins being able to bind directly to PSII intrinsic proteins (Enami et al. 1998, 2003; Nagao et al. 2010a). In particular, in *C. gracilis* the presence of Psb31 alone is described to be able to rebind more than 50% of Cc_{550} as compared with the whole collection of extrinsic proteins (Nagao et al. 2010a). Interestingly, in cyanobacteria Cc_{550} is reported to bind directly to the PSII core, in a manner essentially independent of the other extrinsic proteins, although the binding of Cc_{550} only is not functional (Shen and Inoue 1993; Enami et al. 2003; Nagao et al. 2015). Interestingly, the recent crystal structure of the *C. caldarium* (red alga) PSII has revealed an overall structure similar to the cyanobacterial PSII, which includes the position of Cc_{550} in the complex (Ago et al. 2016).

Previous isolation of *Phaeodactylum* thylakoid-enriched membrane fractions lead to the lack of the five extrinsic subunits of PSII (PsbO, PsbU, PsbQ', Psb31 and PsbV (Grouneva et al. 2011). Here, thylakoid membrane samples containing 35–40 % of the total Cc_{550} could be obtained by lowering the disruption pressure. This amount of membrane-bound cytochrome is in rough agreement with previous studies based in the EPR spectra of Cc_{550} recorded in *T. elongatus* cells, which suggested the presence of a significant concentration of soluble Cc_{550} that could represent between 40–60% of the bound population (Kirilovsky et al. 2004). To further study the Cc_{550} affinity for the PSII core we used a PSII purification method based in sucrose gradient fractioning, in order to preserve as much as possible the PSII integrity, although this method allowed to obtain just PSII-enriched samples, and not purified PSII particles. Consequently, whereas the content in Cc_{550} could be accurately quantified according its spectroscopic properties, the presence of the other subunits can only be followed by Western blot. Therefore, as a control of other PSII extrinsic subunits, PsbO and Psb31 were also monitored and detected in the membrane samples. The low affinity of *Phaeodactylum* Cc_{550} for PSII is demonstrated by the fact that ≈ 90% of Cc_{550} is released through detergent solubilization of the isolated membrane fraction, and thus the protein mostly appears in the upper (not-associated to PSII) gradient fraction

(Figure 3). By contrast, Psb31 remains bound to PSII together with more than 30% of PsbO. It is important to note that similar results were obtained by decreasing the detergent:chlorophyll solubilization ratio and time, although lower PSII extraction and purification yields were then obtained. Thus, our results clearly indicate a low affinity of Cc_{550} for the PSII core, and also that this affinity is lower as compared with some other extrinsic subunits.

It is well known that iron availability limits growth of photosynthetic algae (Moore et al. 2002; Morrissey and Bowler 2012). A down-regulation under iron limitation of several iron-containing proteins has been previously reported in coastal diatoms (Allen et al. 2008; Nunn et al 2013). This down-regulation includes ferredoxin (replaced by flavodoxin), PSI and some subunits of the b_6f complex (Allen et al. 2008; Morrissey and Bowler 2012; Nunn et al. 2013). In *Phaeodactylum*, in particular, PSI and Cc_6 contents are significantly reduced to 30-40% from the values determined under iron-replete conditions (Allen et al. 2008; Roncel et al. 2016). Interestingly, this is also the case of Cc_{550}, for which a decrease of 45-50% in the protein content was determined under iron limitation (Figure 4A). In addition, changing iron availability in cultures acclimated to iron-replete or iron-deplete conditions promoted opposite effects in the Cc_{550} content, *i.e.*: an increase when increasing the iron concentration in the media and a decrease when decreasing iron availability, the adaptation to the new conditions occurring in a time period of 6-8 days (Figure 4B). Actually, our results suggest a similar iron-regulation process for the two main luminal heme proteins, Cc_6 and Cc_{550}, and it is interesting to note that because the different decrease in the protein content for the two cytochromes, under iron limiting conditions the Cc_6/Cc_{550} ratio is reversed.

Acknowledgement

The authors thank Rocío Rodríguez (Proteomic Service, IBVF) for technical assistance, and Prof. Tatsuya Tomo (Tokyo University of Science, Japan) for the Psb31 antibodies.

Supporting Information Available.

REFERENCES

Ago H, Adachi H, Umena Y, Tashiro T, Kawakami K, Kamiya N, Tian L, Han G, Kuang T, Liu Z, Wang F, Zou H, Enami I, Miyano M, Shen J-R (2016) Novel features of eukaryotic photosystem II revealed by its crystal structure analysis from a red alga. J Biol Chem 291:5676–5687

Alam J, Sprinkle MA, Hermodson MA, Krogmann DW (1984) Characterization of cytochrome c-550 from cyanobacteria. Biochim Biophys Acta 766:317–321

Allen AE, Laroche J, Maheswari U, Lommer M, Schauer N, Lopez PJ, Finazzi G, Fernie AR, Bowler C (2008) Whole-cell response of the pennate diatom *Phaeodactylum tricornutum* to iron starvation. Proc Natl Acad Sci USA 105:10438–10443

Alonso PJ, Martínez JI, García-Rubio I (2007) The study of the ground state Kramers doublet of low-spin heminic system revisited. A comprehensive description of the EPR and Mössbauer spectra. Coord Chem Rev 152:12–24

Alonso PJ, Martínez JI (2015) Magnetic properties of a Kramers doublet. An univocal bridge between experimental results and theoretical predictions. J Magn Res 255:1–14

Arnon DI (1949) Copper enzymes in isolated chloroplasts. Plant Physiol 24:1–15

Aro EM, Virgin I, Andersson B (1993) Photoinhibition of Photosystem II. Inactivation, protein damage and turnover. Biochim Biophys Acta 1143:113–134

Bernal-Bayard P, Molina-Heredia FP, Hervás M, Navarro JA (2013) Photosystem I reduction in diatoms: as complex as the green lineage systems but less efficient. Biochemistry 52:8687−8695

Bowler C, Allen AE, Badger JH et al. (2008) The *Phaeodactylum* genome reveals the evolutionary history of diatom genomes. Nature 456, 239–244

Bowler C, Vardi A, Allen AE (2010) Oceanographic and biogeochemical insights from diatom genomes. Ann Rev Mar Sci 2:333–365

Bricker TM, Roose JL, Fagerlund RD, Frankel LK, Eaton-Rye JJ (2012) The extrinsic proteins of Photosystem II. Biochim Biophys Acta 1817:121–142

Bumba L, Havelková-Dousová H, Husák M, Vácha F (2004) Structural characterization of photosystem II complex from red alga *Porphyridium cruentum* retaining extrinsic subunits of the oxygen-evolving complex. Eur J Biochem 271:2967–75

Crimmins DL, Mische SM, Denslow ND (2005) Chemical cleavage of proteins in solution. Curr Protoc Protein Sci, Supp. 41:11.4.1–11

Durán RV, Hervás M, De la Rosa MA, Navarro JA (2005) *In vivo* photosystem I reduction in thermophilic and mesophilic cyanobacteria: The thermal resistance of the process is limited by factors other than the unfolding of the partners. Biochem Biophys Res Commun 334:170–175

Enami I, Iwai M, Akiyama A, Suzuki T, Okumura A, Katoh T, Tada O, Ohta H, Shen J-R (2003) Comparison of binding and functional properties of two extrinsic components, Cyt c_{550} and a 12 kDa protein, in cyanobacterial PSII with those in red algal PSII. Plant Cell Physiol 44:820–827

Enami I, Kikuchi S, Fukuda T, Ohta H, Shen J-R (1998) Binding and functional properties of four extrinsic proteins of photosystem II from a red alga, *Cyanidium caldarium*, as studied by release-reconstitution experiments. Biochemistry 37:2787–2793

Enami I, Murayama H, Ohta H, Kamo M, Nakazato K, Shen J-R (1995) Isolation and characterizaton of a photosystem II complex from a red alga *Cyanidium caldarium*: association of cytochrome *c*-550 and a 12 kDa protein with the complex. Biochim Biophys Acta 1232:208–216

Enami I, Okumura A, Nagao R, Suzuki T, Iwai M, Shen J-R (2008) Structures and functions of the extrinsic proteins of photosystem II from different species. Photosynth Res 98: 349–363

Evans PK, Krogmann DW (1983) Three c-type cytochromes from the red alga *Porphyridium cruentum*. Arch Biochem Biophys 227:494–510

Ferreira KN, Iverson TM, Maghlaoui K, Barber J, Iwata S (2004) Architecture of the photosynthetic oxygen evolving center. Science 303:1831–1838

Frazão C, Enguita FJ, Coelho R, Sheldrick GM, Navarro JA, Hervás M, De la Rosa MA, Carrondo MA (2001) Crystal structure of low-potential cytochrome c_{549} from *Synechocystis* sp. PCC 6803 at 1.21 Å resolution. J Biol Inorg Chem 6:324–332

García-Rubio I, Martínez JI, Picorel R, Yruela I, Alonso PJ (2003) HYSCORE spectroscopy in the cytochrome b(559) of the photosystem II reaction center. J Am Chem Soc 125:15846–15854

Goldman JC, McCarthy JJ (1978) Steady state growth and ammonium uptake of a fast-growing marine diatom 1. Limnol Oceanogr 23:695–703

Griffith JS (1957) Theory of electron resonance in ferrihaemoglobin azide. Nature 180:30–31

Grouneva I, Gollan PJ, Kangasjärvi S, Suorsa M, Tikkanen M, Aro E-M (2013) Phylogenetic viewpoints on regulation of light harvesting and electron transport in eukaryotic photosynthetic organisms. Planta 237:399–412

Grouneva I, Rokka A, Aro E-M (2011) The thylakoid membrane proteome of two marine diatoms outlines both diatom-specific and species-specific features of the photosynthetic machinery. J Proteome Res 10:5338–5353

Guerrero F, Sedoud A, Kirilovsky D, Rutherford AW, Ortega JM, Roncel M (2011) A high redox potential form of cytochrome c_{550} in Photosystem II from *Thermosynechococcus elongatus*. J Biol Chem 286:5985–5894

Guerrero F, Zurita JL, Roncel M, Kirilovsky D, Ortega JM, (2014) The role of the high potential form of the cytochrome b_{559}: study of *Thermosynechococcus elongatus* mutants. Biochim Biophys Acta 1837:908–919

Guex N, Peitsch MC (1997) SWISS-MODEL and the Swiss-PdbViewer: an environment for comparative protein modelling. Electrophoresis 18:2714–2723

Haehnel W, Ratajczak R, Robenek H (1989) Lateral distribution and diffusion of plastocyanin in chloroplast thylakoids. J Cell Biol 108:1397–1405

Ifuku K, Noguchi T (2016) Structural coupling of extrinsic proteins with the oxygen-evolving center in photosystem II. Front Plant Sci 7:84

Ioanitescu AI, Van Doorslaer S, Dewilde S, Endeward B, Moens L (2007) Probing the heme-pocket structure of the paramagnetic forms of cytoglobin and a distal histidine mutant using electron paramagnetic resonance. Molecular Physics 105:2073–2086

Jeffrey S, Humphrey G (1975) New spectrophotometric equations for determining chlorophylls a, b, c1 and c2 in higher plants, algae and natural phytoplankton. Biochem Physiol Pflanzen 167:191–194

Kang C, Chitnis RP, Smith S, Krogmann DW (1994) Cloning and sequence analysis of the gene encoding the low potential cytochrome c of *Synechocystis* PCC 6803. FEBS Lett 344:5–9

Kato Y, Sakamoto W (2010) New insights into the types and function of proteases in plastids. Int Rev Cell Mol Biol 280, Chapter 4:185–218

Kelley LA, Sternberg MJE (2009) Protein structure prediction on the web: a case study using the Phyre server. Nat Protoc 4:363–371

Kerfeld CA, Krogmann DW (1998) Photosynthetic cytochromes c in cyanobacteria, algae and plants. Annu Rev Plant Physiol Plant Mol Biol 49:397–425

Kerfeld CA, Sawaya MR, Bottin H, Tran KT, Sugiura M, Cascio D, Desbois A, Yeates TO, Kirilovsky D, Boussac A (2003) Structural and EPR characterization of the soluble form of cytochrome c-550 and of the *psbV2* gene product from the cyanobacterium *Thermosynechococcus elongatus*. Plant Cell Physiol 44:697–706

Key T, McCarthy A, Campbell DA, Six C, Roy S, Finkel ZV (2010) Cell size trade-offs govern light exploitation strategies in marine phytoplankton. Environ Microbiol 12:95–104

Kienzel PF, Peschek GA (1983) Cytochrome c-549: an endogenous cofactor of cyclic photophosphorylation in the cyanobacterium *Anacystis nidulans*. FEBS Lett 162:76–80

Kirilovsky D, Roncel M, Boussac A, Wilson A, Zurita JL, Ducruet JM, Bottin H, Sugiura M, Ortega JM, Rutherford AW (2004) Cytochrome c_{550} in the cyanobacterium *Thermosynechococcus elongatus*: study of redox mutants. J Biol Chem 279:52869–52880

Kooistra WHCF, Gersonde R, Medlin LK, Mann DG. The origin and evolution of the diatoms: their adaptation to a planktonic existence. In: Evolution of Primary Producers in the Sea (Falkowski PG and Knoll AH, eds.), 2007 Academic Press Inc., pp. 207–249

Krogmann DW (1991) The low-potential cytochrome c of cyanobacteria and algae. Biochim Biophys Acta 1058:35–37

Lavaud J, Six C, Campbell DA (2016) Photosystem II repair in marine diatoms with contrasting photophysiologies. Photosynth Res 127:189–199

Loll B, Kern J, Saenger W, Zouni A, Biesiadka J (2005) Towards complete cofactor arrangement in the 3.0 Å resolution structure of photosystem II. Nature 438:1040–1044

Martínez-Fábregas J, Díaz-Moreno I, González-Arzola K, Janocha S, Navarro JA, Hervás M, Bernhardt R, Velázquez-Campoy A, Díaz-Quintana A, De la Rosa MA (2014) Structural and functional analysis of novel human cytochrome *c* targets in apoptosis. Mol Cell Proteomics 13:1439–1456

Martinson TA, Ikeuchi M, Plumley FG (1998) Oxygen-evolving diatom thylakoid membranes. Biochim Biophys Acta 1409:72–86

McLachlan J (1964) Some considerations of the growth of marine algae in artificial media. Can J Microbiol 10:769–782

Molina-Heredia FP, Hervás M, Navarro JA, De la Rosa Acosta MA (1998) Cloning and correct expression in *Escherichia coli* of the *petE* and *petJ* genes respectively encoding plastocyanin and cytochrome c_6 from the cyanobacterium *Anabaena* sp. PCC 7119. Biochem Biophys Res Commun 243:302–306

Moore JK, Doney SC, Glover DM, Fung IY (2002) Iron cycling and nutrient-limitation patterns in surface waters of the World Ocean. Deep Sea Res II 49:463–507

Morand LZ, Cheng RH, Krogmann DW (1994) Soluble electron transfer catalysts of cyanobacteria. In: The Molecular Biology of Cyanobacteria (Bryant DA, ed.). Kluwer Academic Publishers, Dordrecht, pp. 381–407

Morrissey J, Bowler C (2012) Iron utilization in marine cyanobacteria and eukaryotic algae. Front Microbiol 3:1–13

Nagao R, Ishii A, Tada O, Suzuki T, Dohmae N, Okumura A, Iwai M, Takahashi T, Kashino Y, Enami I (2007) Isolation and characterization of oxygen-evolving thylakoid membranes and Photosystem II particles from a marine diatom *Chaetoceros gracilis.* Biochim Biophys Acta 1767:1353–1362

Nagao R, Moriguchi A, Tomo T, Niikura A, Nakajima S, Suzuki T, Okumura A, Iwai M, Shen J-R, Ikeuchi M, Enami I (2010a) Binding and functional properties of five extrinsic proteins in oxygen-evolving photosystem II from a marine centric diatom, *Chaetoceros gracilis.* J Biol Chem 285:29191–29199

Nagao R, Tomo T, Noguchi E, Nakajima S, Suzuki T, Okumura A, Kashino Y, Mimuro M, Ikeuchi M, Enami I (2010b) Purification and characterization of a stable oxygen-evolving Photosystem II complex from a marine centric diatom, *Chaetoceros gracilis*. Biochim Biophys Acta 1797:160–166

Nagao R, Tomo T, Narikawa R, Enami I, Ikeuchi M (2013) Light-independent biosynthesis and assembly of the photosystem II complex in the diatom *Chaetoceros gracilis*. FEBS Lett 587:1340–1345

Nagao R, Tomo T, Narikawa R, Enami I, Ikeuchi M (2016) Conversion of photosystem II dimer to monomers during photoinhibition is tightly coupled with decrease in oxygen-evolving activity in the diatom *Chaetoceros gracilis*. Photosynth Res 130:83–91

Nagao R, Tomo T, Noguchi E (2015) Effects of extrinsic proteins on the protein conformation of the oxygen-evolving center in cyanobacterial photosystem II as revealed by Fourier transform infrared spectroscopy. Biochemistry 54:2022–2031

Nagao R, Tomo T, Noguchi E, Suzuki T, Okumura A, Narikawa R, Enami I, Ikeuchi M (2012) Proteases are associated with a minor fucoxanthin chlorophyll *a/c*-binding protein from the diatom *Chaetoceros gracilis*. Biochim Biophys Acta 1817:2110–2117

Navarro JA, Hervás M, De la Cerda B, De la Rosa MA (1995) Purification and physicochemical properties of the low potential cytochrome c_{549} from the cyanobacterium *Synechocystis* sp. PCC 6803. Arch Biochem Biophys 3186:46–52

Navarro JA, Hervás M, De la Rosa MA. Purification of plastocyanin and cytochrome c_6 from plants, green algae, and cyanobacteria. In: Photosynthesis Protocols (Carpentier R ed.) 2011, vol. 684, Humana Press, Totowa, NJ, USA, pp 79–94

Nunn BL, Faux JF, Hippmann AA, Maldonado MT, Harvey HR, Goodlett DR, Boyd PW, Strzepek RF (2013) Diatom proteomics reveals unique acclimation strategies to mitigate Fe limitation. PLoS ONE 8, e75653:1–16

Okumura A, Nagao R, Suzuki T, Yamagoe S, Iwai M, Nakazato K, Enami I (2008) A novel protein in Photosystem II of a diatom *Chaetoceros gracilis* is one of the extrinsic proteins located on lumenal side and directly associates with PSII core components. Biochim Biophys Acta 1777:1545–1551

Peisach J, Blumberg WE, Adler A (1973) Electron paramagnetic resonance studies of iron porphin and chlorin systems. Ann New York Ac Sci 206:310–327

Quinn R, Valentine JS, Byrn MP, Strouse CE (1987) Electronic-structure of low-spin ferric porphyrins: A single-crystal EPR and structural investigation of the influence of axial ligand orientation and the effects of pseudo-Jahn-Teller distortion. J Am Chem Soc 109:3301-3308

Roncel M, Boussac A, Zurita JL, Bottin H, Sugiura M, Kirilovsky D, Ortega JM (2003) Redox properties of the photosystem II cytochromes b_{559} and c_{550} in the cyanobacterium *Thermosynechococcus elongatus*. J Biol Inorg Chem 8:206–216

Roncel M, González-Rodríguez AA, Naranjo B, Bernal-Bayard P, Lindahl AM, Hervás M, Navarro JA, Ortega JM (2016) Iron deficiency induces a partial inhibition of the photosynthetic electron transport and a high sensitivity to light in the diatom *Phaeodactylum tricornutum*. Front Plant Sci 7:1050

Roncel M, Kirilovsky D, Guerrero F, Serrano A, Ortega JM (2012) Photosynthetic cytochrome c_{550}. Biochim Biophys Acta 1817:1152–1163

Sawaya MR, Krogmann DW, Serag A, Ho KK, Yeates TO, Kerfeld CA (2001) Structures of cytochrome c-549 and cytochrome c6 from the cyanobacterium *Arthrospira maxima*. Biochemistry 40:9215–9225

Schweiger A, Jeschke G. Principles of pulse electron paramagnetic resonance. Oxford University Press, 2001

Sechi S, Chait BT (1998) Modification of cysteine residues by alkylation. A tool in peptide mapping and protein identification. Anal. Chem. 70:5150–5158

Shen J-R (2015) The structure of photosystem II and the mechanism of water oxidation in photosynthesis. Annu Rev Plant Biol 66:23–48

Shen J-R, Inoue Y (1993) Binding and functional properties of two new extrinsic components, cytochrome c-550 and a 12-kDa protein, in cyanobacterial photosystem II. Biochemistry 32:1825–1832

Shen J-R, Qian M, Inoue Y, Burnap RL (1998) Functional characterization of *Synechocystis* sp. 6803 ΔpsbU and ΔpsbV mutants reveals important roles of cytochrome c-550 in cyanobacterial oxygen evolution. Biochemistry 37:1551–558

Shimazaki K, Takamiya K, Nishimura M (1978) Studies on electron transfer systems in the marine diatom *Phaeodactylum tricornutum*. I. Isolation and characterization of cytochromes. J Biochem 83:1631–1638

Suga M, Lai T-L, Sugiura M, Shen J-R, Boussac A (2013) Crystal structure at 1.5 Å resolution of the PsbV2 cytochrome from the cyanobacterium *Thermosynechococcus elongatus*. FEBS Lett 587:3267–3272

Takaoka T, Sakashita N, Saito K, Ishikita H (2016) pKa of a proton-conducting water chain in photosystem II. J Phys Chem Lett 7:1925–1932

Taylor CPS (1977) The EPR of low spin heme complexes. Relation of the t2g hole model to the directional properties of the g tensor, and a new method for calculating the ligand field parameters. Biochim Biophys Acta 491:137–149

Umena Y, Kawakami K, Shen J-R, Kamiya N (2011) Crystal structure of oxygen-evolving photosystem II at a resolution of 1.9 Å. Nature 473:55–60

Van Doorslaer S, Tilleman L, Verrept B, Dewilde S (2012) Marked difference in the electronic structure of cyanide-ligated ferric protoglobins and myoglobin due to heme ruffling. Inorg Chem 51:8834–8841

Vogt L, Vinyard DJ, Khan S, Brudvig GW (2015) Oxygen-evolving complex of Photosystem II: an analysis of second-shell residues and hydrogen-bonding networks. Curr Opin Chem Biol 25:152–158

Vrettos JS, Reifler MJ, Kievit O, Lakshmi KV, Lakshmi JC, de Paula JC, Brudvig GW (2001) Factors that determine the unusually low reduction potential of cytochrome c_{550} in cyanobacterial photosystem II. J Biol Inorg Chem 6:708–716

Walker FA, Huynh BH, Scheidt WR, Osvath RS (1986) Models of the cytochromes *b*. Effect of axial ligand plane orientation on the EPR and Mössbauer spectra of low-spin ferrihemes. J Am Chem Soc 108:5288–5297

Wu H, Cockshutt AM, McCarthy A, Campbell DA (2011) Distinctive photosystem II photoinactivation and protein dynamics in marine diatoms. Plant Physiol 156:2184–2195

Yruela I, García-Rubio I, Roncel M, Martínez JI, Ramiro MV, Ortega JM, Alonso PJ, Picorel R (2003) Detergent effect on cytochrome b_{559} electron paramagnetic resonance signals in the photosystem II reaction centre. Photochem Photobiol Sci 2:437–442

Zouni A, Witt HT, Kern J, Fromme P, Kraub N, Saenger W, Orth P (2001) Crystal Structure of oxygen evolving Photosystem II from *Synechococcus elongatus* a 3.8 Å resolution. Nature 409:739–743

TABLE 1. Comparison of EPR parameters of Cc_{550} from *P. tricornutum* and other species

	g_z	g_y	g_x	Δ/λ	V/λ	V/Δ	pdb code
Soluble Cc_{550}							
P. tricornutum	3.00	2.24	1.44	3.17	1.71	0.54	-
A. nidulans[a]	2.98	2.24	1.46	3.22	1.75	0.54	-
T. elongatus[a]	2.97	2.24	1.49	3.35	1.80	0.54	1MZ4
A. maxima[b]	2.90	2.27	1.54	3.29	1.97	0.60	1F1C
Synechocystis 6803[a,c]	2.87	2.28	1.57	3.32	2.06	0.62	1E29
PSII-bound Cc_{550}							
T. elongatus[a]	3.02	2.20	1.45	3.46	1.68	0.48	4V62, 2AXT
Synechocystis 6803[c]	2.88	2.23	1.50	3.28	1.91	0.58	-

[a]Values reported by Kerfeld et al. (2003); [b]Values reported by Sawaya et al. (2001); [c]Values reported by Vrettos et al. (2001).

FIGURE LEGENDS

Figure 1. Different purification and protein extraction procedures carried out during the characterization of Cc_{550} from the diatom *Phaeodactylum tricornutum*. Asterisks indicate samples analyzed by MALDI-TOF in Figure 2. See text for further details.

Figure 2. (*Upper*) Molecular weight MS-analysis of different samples obtained during the purification of Cc_{550} from *Phaeodactylum tricornutum*. (A) Cc_{550} purified from the soluble cell extract; the peak on the left corresponds to the Cc_{550} main peak at z = 2. (B) Clarified crude extract obtained after treatment with streptomycin sulfate and sequential precipitation with ammonium sulfate. (C) Cc_{550} sample obtained from the salt-detergent washing of the membrane fraction. (*Lower*) Protein sequence of *Phaeodactylum* Cc_{550} as translated from the *psbV* gene, and theoretical MW of the complete protein or different truncated forms. See the Experimental Procedures section for further information.

Figure 3. (*Upper*) Western blot analysis of the different fractions acquired along the obtention of PSII-enriched samples from *Phaeodactylum tricornutum* as indicated in Figure 1 (M, molecular weight standard). Cc_{550} and both the D1 core and the PsbO and Psb31 extrinsic subunits of PSII were observed. For a comparative monitoring of each protein in the different fractions, in lines 1-4 equivalent sample volumes were loaded related to the initial volume of crude extract, whereas in lines 5-6 equivalent volumes related to the volume of the fractions directly extracted from the sucrose gradient bands were loaded. (*Lower*) Spectroscopic monitoring of cytochrome b_{559} (Cb_{559}) of PSII (ascorbate *minus* ferricyanide, continuous line) and Cc_{550} (dithionite *minus* ascorbate, dashed line) in: (5) the top of the gradient, and (6) the lower green band in the sucrose gradient. PSII was monitored by the absorbance changes corresponding to cytochrome b_{559}.

Figure 4. (A,C) Content of (A) Cc_{550} and (C) Cc_6 in *Phaeodactylum tricornutum* cultures grown under iron-replete or iron-deplete conditions, as indicated, estimated by the specific redox differential absorbance changes (dithionite *minus* ascorbate or ascorbate *minus* ferricyanide, respectively). (A, *inset*) Expanded spectra in the region of the Cc_{550} α-band. (B,D) Variations in (B) Cc_{550} and (D) Cc_6 content of cultures after changing iron availability. Cells growing in iron-replete (○) or iron-deficient (□) media, were resuspended in the same

fresh medium; (■) cells growing in iron-deficient medium were resuspended in fresh iron-replete medium; (●) cells growing in iron-replete medium were resuspended in fresh iron-deficient medium. See the Experimental Procedures section for further information.

Figure 5. EPR spectra of Cc_{550} from *Phaeodactylum tricornutum.* (A) CW-EPR spectrum taken at T = 25 K. (B) Echo-detected EPR, T = 6 K, π = 96 ns. (C) Hole model. Energy levels of the t_{2g} orbitals in C2v symmetry and definition of the parameters Δ and V. (D) HYSCORE performed at the magnetic field corresponding to g_z (B = 230 mT). τ = 96 ns, T = 8.5 K. Double-quantum correlation peaks are indicated with arrows.

Figure 6. (A) Backbone model of Cc_{550} from *Phaeodactylum tricornutum* obtained using the program Phyre[2], with the crystal structures of Cc_{550} from the cyanobacteria *Thermosynechococcus elongatus* (pdb 1MZ4) and *Synechocystis* sp. PCC 6803 (pdb 1E29) as main templates. (B-E) Surface electrostatic potential distribution of the structural model of Cc_{550} from *Phaeodactylum* either in (B) the complete and (C) truncated forms, (D) *Synechocystis* 6803 and (E) the red alga *Cyanidium caldarium* (pdb 4YUU). The view displays the heme groups in the same orientation, showing in front the cofactor exposed area and in the top the protein C-terminal part. Simulations of surface electrostatic potential distribution were performed using the Swiss-Pdb Viewer Program assuming an ionic strength of 500 mM at pH 7.0. Positively and negatively charged regions are depicted in blue and red, respectively.

Figure 7. Detail of surface electrostatic potential distribution around the heme group of Cc_{550} from: (A) *Phaeodactylum tricornutum* (model shown in Figure 6C), (B) *Termosynechoccocus elongatus* (pdb 1MZ4), (C) *Arthrospira maxima* (pdb 1F1C) and (D) *Synechocystis* sp. PCC 6803 (pdb 1E29). The view shows in front the heme group exposed area. Positively and negatively charged regions are depicted in blue and red, respectively. The same view of the entrance to the heme pocket is displayed for *T. elongatus*, *Synechocystis* 6803 and *A. maxima* structures and for the *Phaeodactylum* model. See Figure 6 for further details.

Supplementary Material.

Figure S1. Absorption spectra of Cc_{550} (10 μM) from *Phaeodactylum tricornutum* is its native oxidized form (continuous line) and after reduction with dithionite (dashed line). (*Inset*) Reductive potentiometric redox titration of purified Cc_{550} (10 μM) in potassium phosphate 50 mM, pH 7, buffer. Continuous line corresponds to the theoretical fit according the Nernst equation and n = 1. See the Experimental Procedures section for further information.

Figure S2. BrCN cleavage and peptide analysis of Cc_{550} from *Phaeodactylum tricornutum*. (*Upper*) Theoretical protein sequence as deduced from the translation of the *psbV* gene. Methionine targets for BrCN are underlined. (*Middle*) Molecular weight MS-analysis of the different peptides obtained during the BrCN digestion of Cc_{550}. Arrows indicate the peptides fitting the expected results from the digestion of the truncated Cc_{550}. (*Lower*) Expected main peptides from the Cc_{550} cleavage by BrCN in methionine positions, either in the theoretical protein (1-3) or the truncated form (1,2,4,5). Peptide 3 was not detected.

Figure S3. (*Left*) Cc_{550} and (*right*) Cc_6 content in the soluble fraction (continuous line) of *Phaeodactylum tricornutum* disrupted cells, and in samples obtained after treating the membrane fractions with NaCl and detergent (dashed line), as estimated from the differential absorbance spectra (reduced *minus* oxidized). See the Experimental Procedures section for further information.

Figure S4. Sequence alignment of Cc_{550} from *Phaeodactylum tricornutum*, *Termosynechoccocus elongatus*, *Arthrospira maxima* and *Synechocystis* sp. PCC 6803. Arrows point to the axial heme histidine ligands.

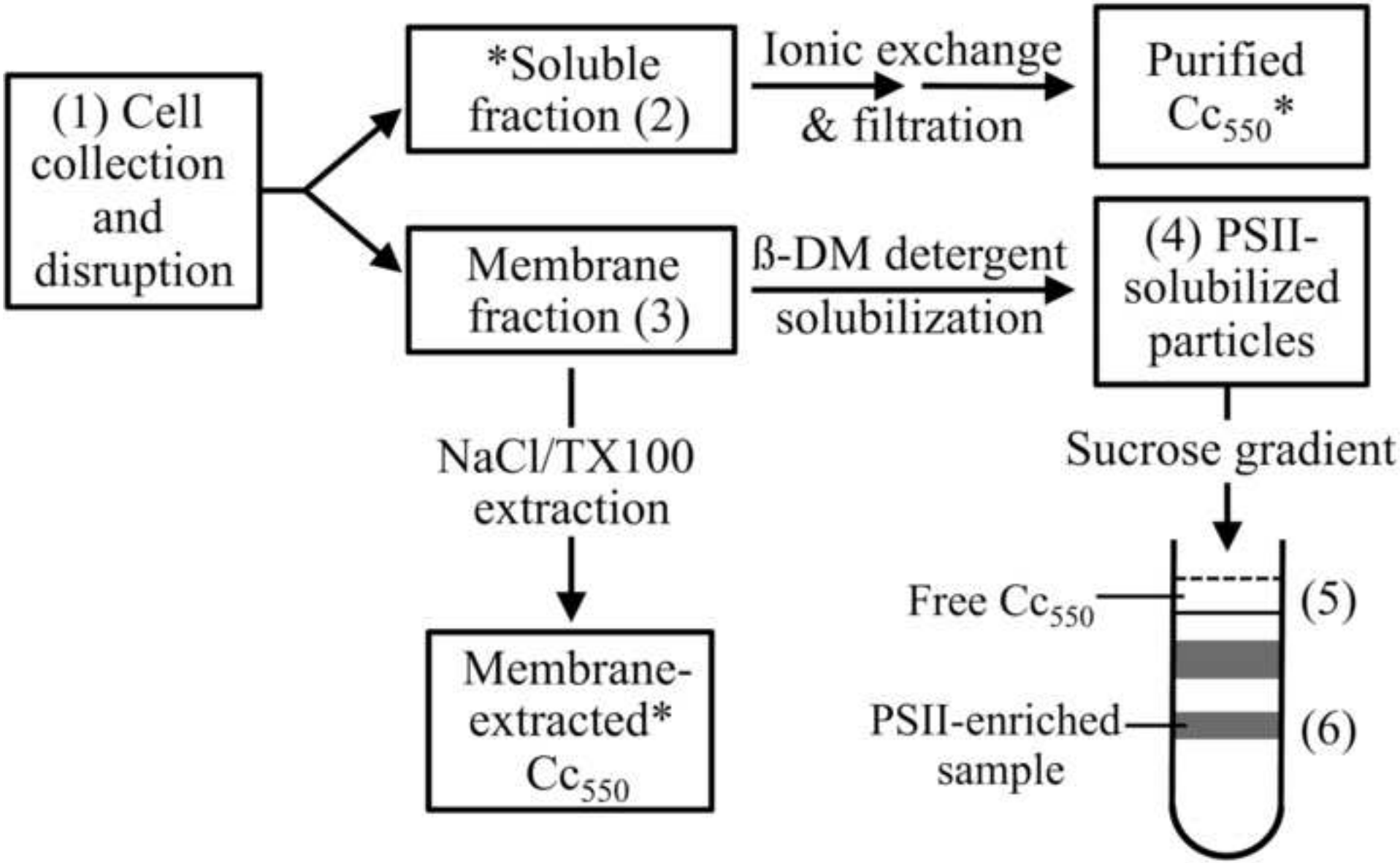
(1) Cell collection and disruption
*Soluble fraction (2)
Ionic exchange & filtration
Purified Cc_{550}*
Membrane fraction (3)
ß-DM detergent solubilization
(4) PSII-solubilized particles
NaCl/TX100 extraction
Sucrose gradient
Membrane-extracted* Cc_{550}
Free Cc_{550}
(5)
PSII-enriched sample
(6)

Figure 1

Figure 2

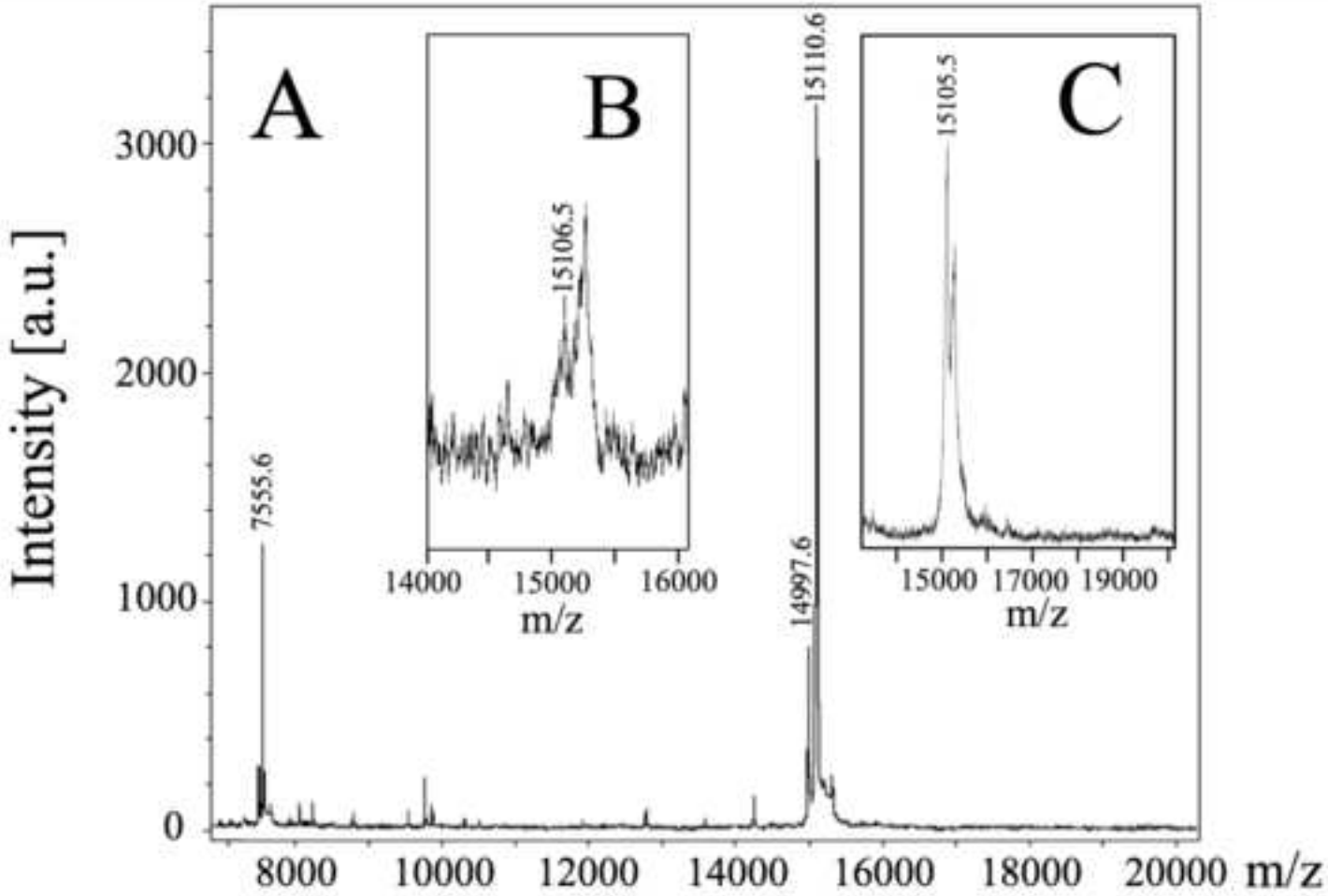

IDLDEATRTV VVDSSGKTIV LTPEQVKRGK RLFNATCGAC
HVGGVTKTNP NVGLDPEALS LATPRRDNIA GLVDFLKNPT
TYDGLESIAE VHPSIKSADI YPRMRSVTDE DLTAMAGHIL

LQPKIVTEKW GGGKIYY	**MW = 15,438; *psbV* gene sequence**
LQPKIVTEKW GGGKI	**MW = 15,111; truncated 2-C-terminal**
LQPKIVTEKW GGGK	**MW = 14,998; truncated 3-C-terminal**

Figure 3

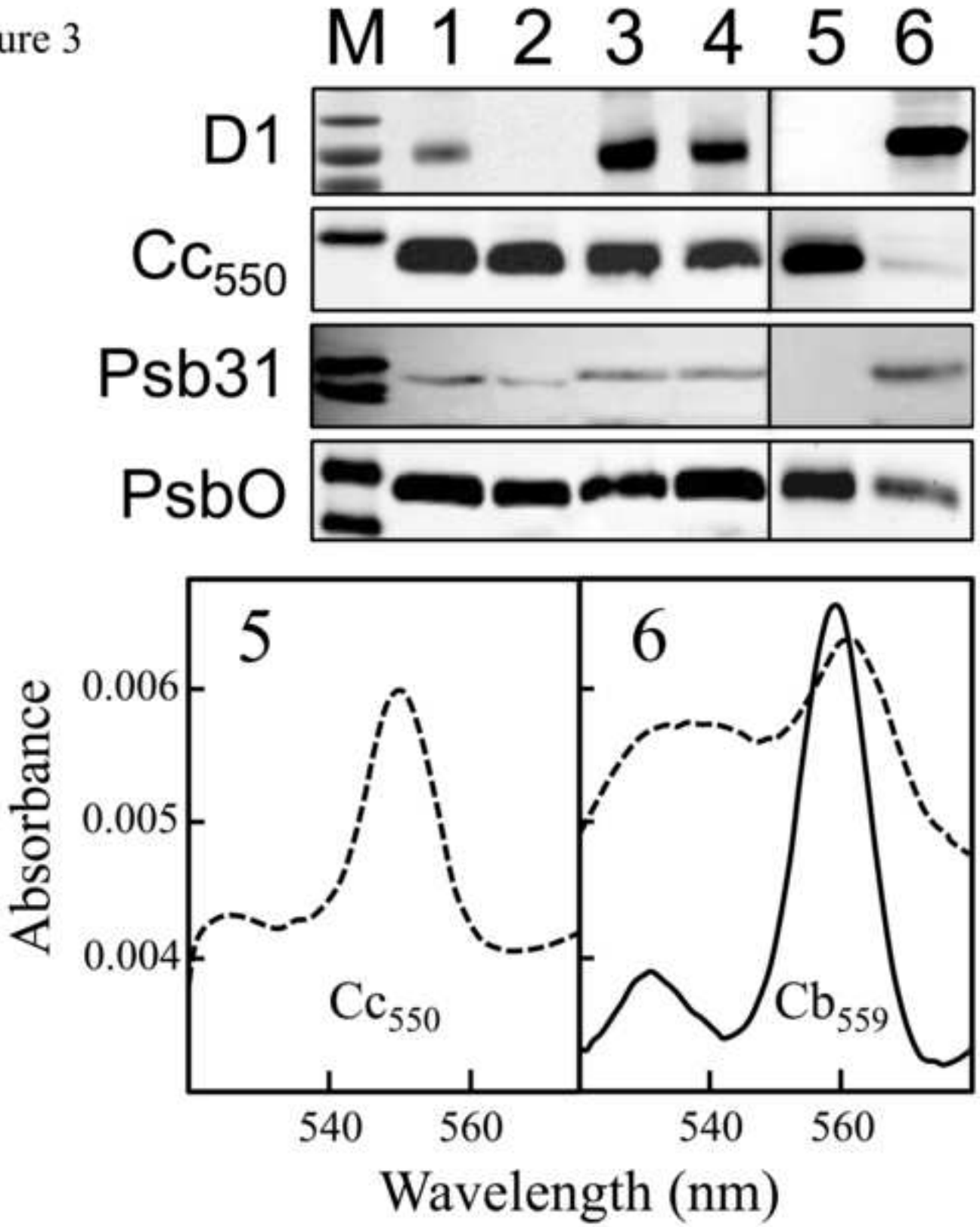

Figure 4

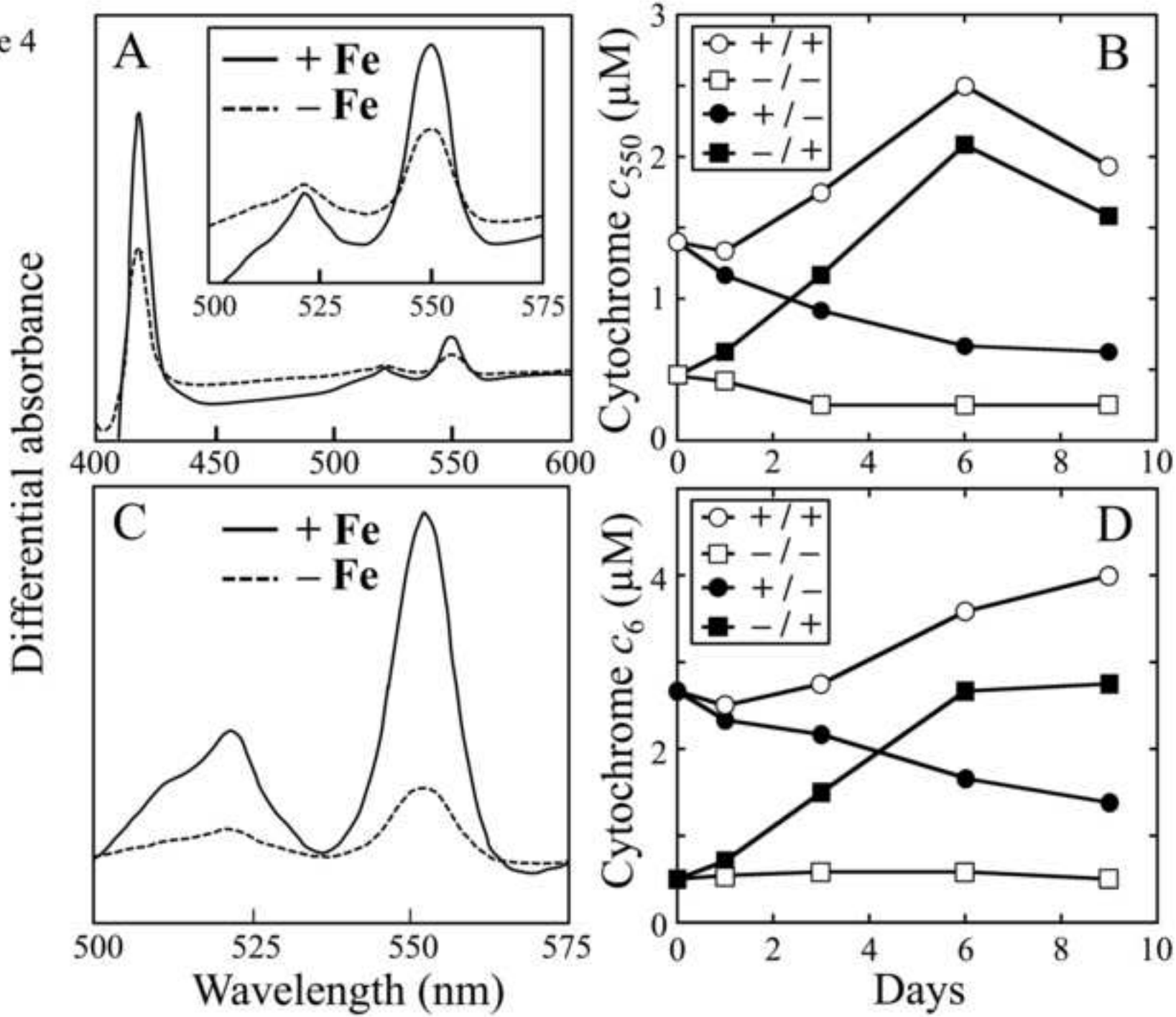

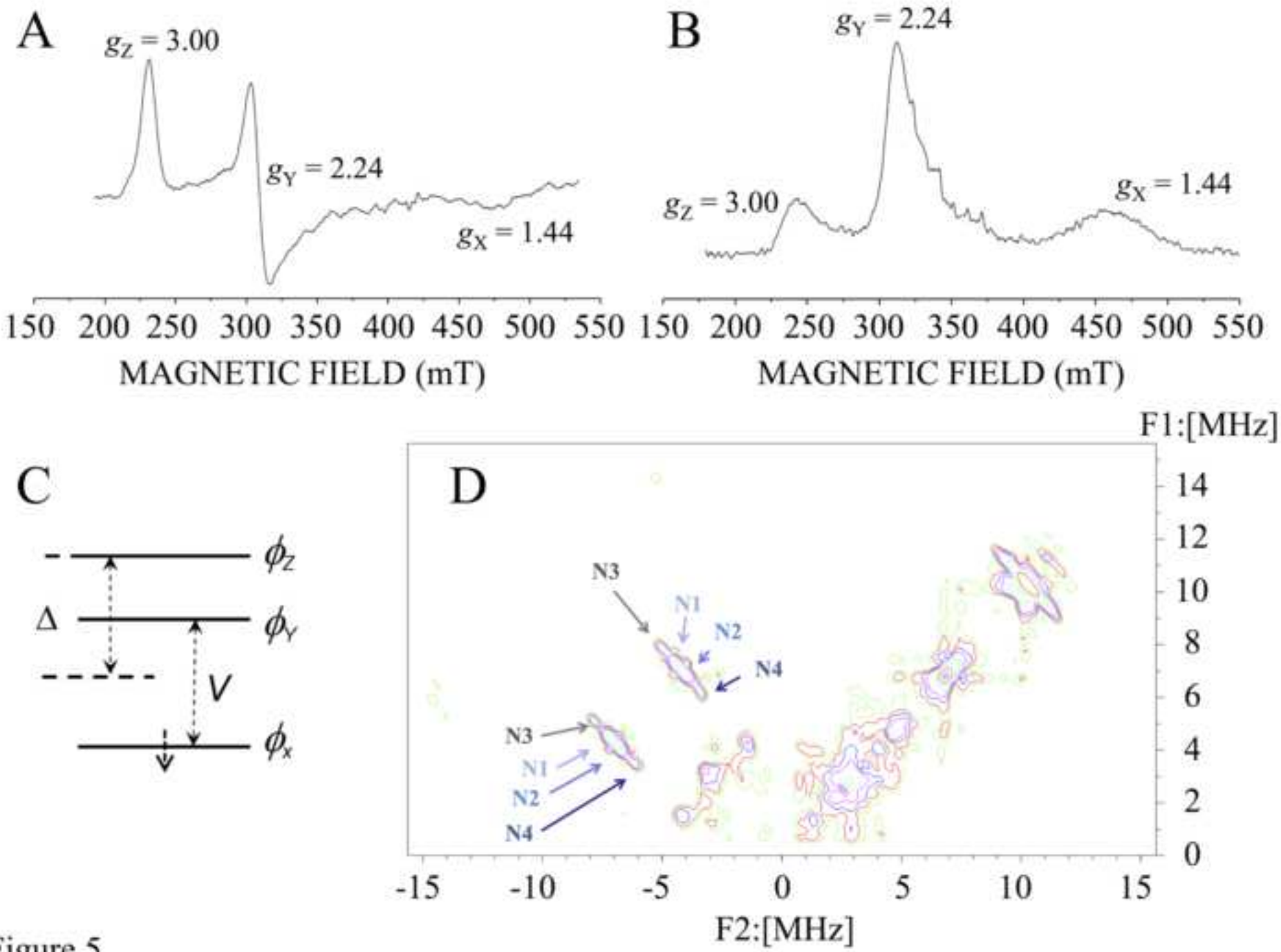

Figure 5

Figure 6

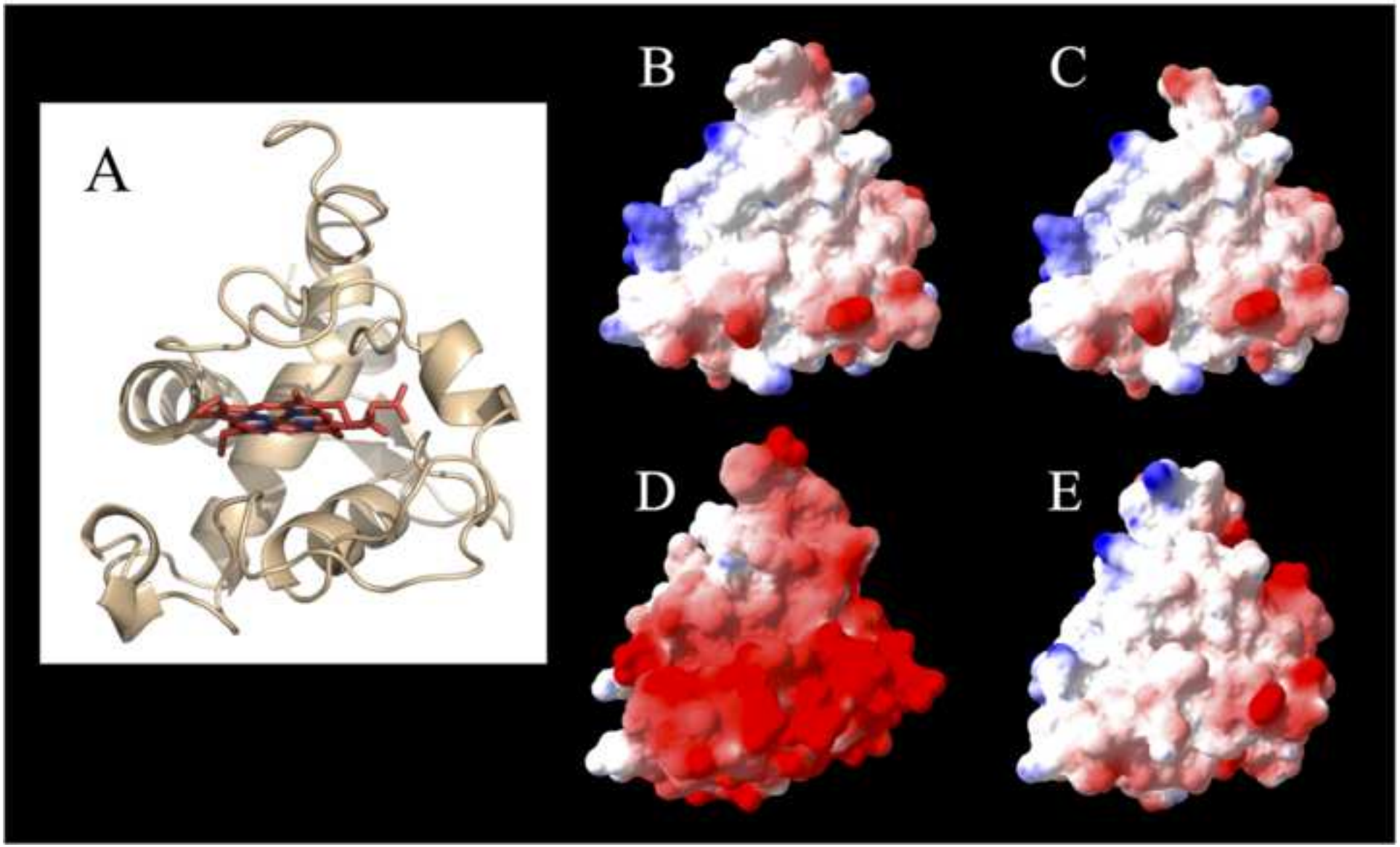

Figure 7

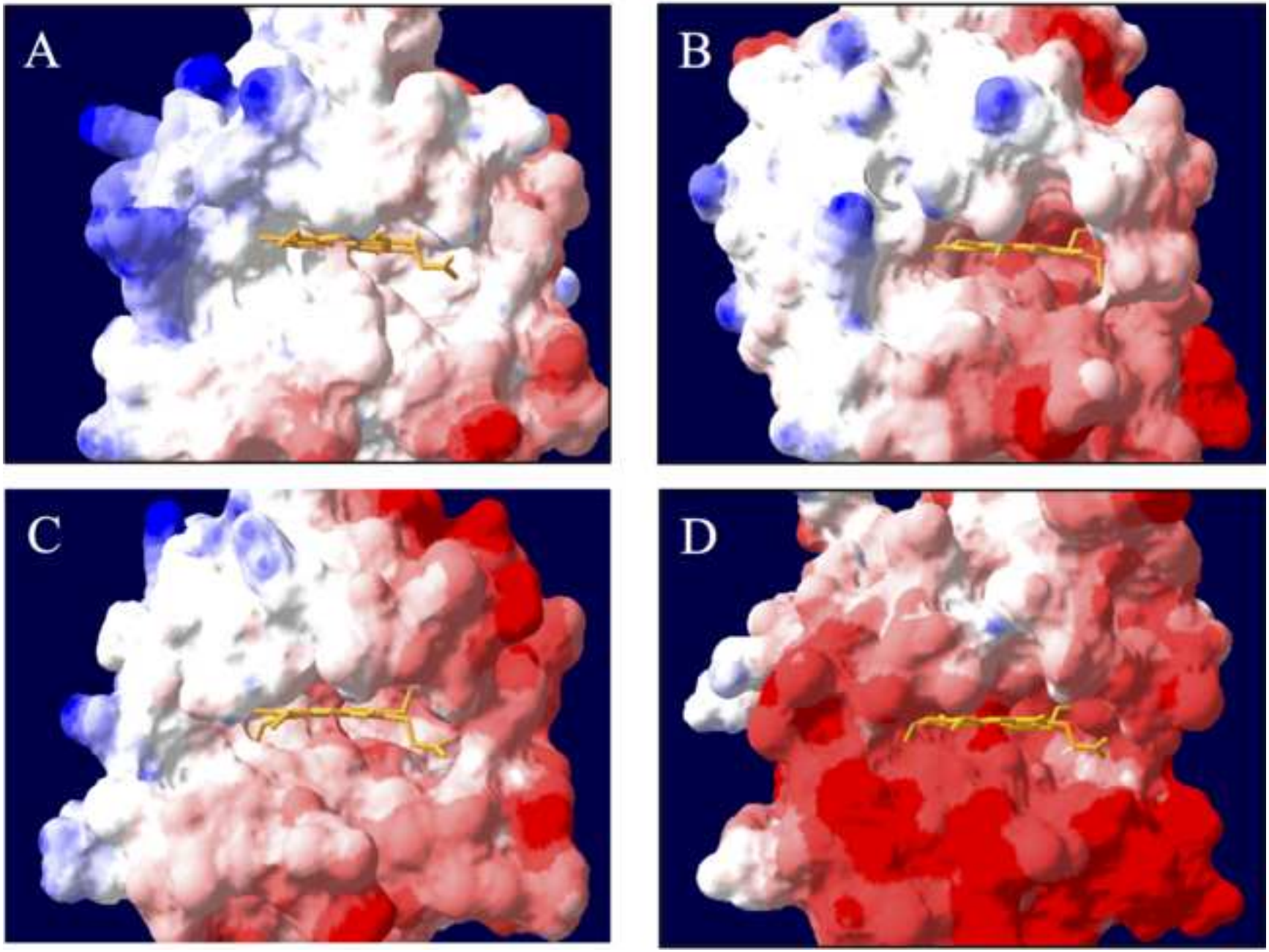

Figure S1

Figure S2

Figure S3

Figure S4